Microporous and Mesoporous Materials 136 (2010) 50–58

Contents lists available at ScienceDirect

Microporous and Mesoporous Materials

journal homepage: www.elsevier.com/locate/micromeso

Methane storage mechanism in the metal-organic framework $Cu_3(btc)_2$: An *in situ* neutron diffraction study

Juergen Getzschmann [a], Irena Senkovska [a], Dirk Wallacher [b], Michael Tovar [b], David Fairen-Jimenez [c], Tina Düren [c], Jasper M. van Baten [d], Rajamani Krishna [d], Stefan Kaskel [a,*]

[a] Department of Inorganic Chemistry, Dresden University of Technology, Germany
[b] Helmholtz Centre Berlin for Materials and Energy, Berlin, Germany
[c] Institute for Materials and Processes, School of Engineering, The University of Edinburgh, United Kingdom
[d] Van 't Hoff Institute for Molecular Sciences, University of Amsterdam, The Netherlands

ARTICLE INFO

Article history:
Received 4 May 2010
Received in revised form 27 July 2010
Accepted 29 July 2010
Available online 11 August 2010

Keywords:
HKUST-1
Molecular simulation
Deutero-methane adsorption
Neutron powder diffraction
Adsorption site

ABSTRACT

The adsorption of deutero-methane (CD_4) in $Cu_3(btc)_2$ (HKUST-1) was investigated at 77 K using high-resolution neutron powder diffraction. Rietveld refinement of the neutron data revealed a sequential filling of the rigid framework at distinct preferred adsorption sites, and showed the importance of open metal sites even for non-polar molecules such as methane. Four main adsorption sites were identified, located inside the small and two larger pores of the framework. The shorter distances between the CD_4 center and the pore wall atoms are covering a range from 3.07 to 3.547 Å. The maximum occupation of 170 CD_4 molecules per unit cell, estimated from the refined occupancy of the adsorption sites, is close to the value estimated from volumetric adsorption isotherms at 77 K (176 molecules per cell). Molecular simulation gave further insight into the adsorption mechanism.

1. Introduction

Recently metal-organic frameworks (MOFs) have received considerable attention for applications in gas storage by adsorption [1–4]. Due to the high specific surface area and pore volume exceeding some of the traditional adsorbents such as zeolites and activated carbons MOFs have very high capacities for hydrogen at 77 K [5–7]. The higher heat of adsorption for methane allows the storage of significant amounts even at room temperature. However, the interaction is still weak enough to guarantee full reversibility of the storage process. Adsorptive gas storage in MOFs can thus increase the volumetric tank capacity at 300 K by a factor of up to 2.5 compared to an empty tank [8]. While the number of methane adsorption studies on MOFs by physisorption is high, there is still only little insight in the mechanisms and location of methane molecules inside MOFs [9]. Here, *in situ* diffraction studies are a valuable tool as they allow determining the location of adsorbed molecules in the framework at low temperatures. This technique has been successfully applied to study the adsorption of gases in zeolites and more recently has been extended to study the adsorption of hydrogen in MOFs [10–14]. Thus for MOF-5, [12] $Cu_3(btc)_2$ (btc = 1,3,5-benzene tricarboxylate) [10–12], $Cu_3[Co(CN)_6]_2$ [13,14] and $Mn_3[(Mn_4Cl)_3(btt)CH_3OH)_{10}]_2$ (btt = 1,3,5-benzene tristetrazolate)[12] hydrogen (or deuterium, D_2) was located by neutron diffraction. The latter two materials exhibit open metal sites inside the pore and neutron studies have revealed a preferred adsorption of hydrogen at these centres. Even though such open metal adsorption sites seem to have a higher adsorption enthalpy (up to -12 kJ mol^{-1}), due to their limited number they only play a significant role at low surface coverage, whereas at levels reaching meaningful capacities the enthalpies seem to approach -5 to -6 kJ mol^{-1}.

So far, only one study was dedicated to the *in situ* observation of methane in a MOF using neutron diffraction [15]. In our contribution, we report for the first time the location of CD_4 in $Cu_3(btc)_2$ determined by neutron diffraction and molecular simulation in order to get a deeper insight into the adsorption mechanism. Moreover, we demonstrate the existence of preferential adsorption sites at the open metal positions for methane, a highly symmetric, non-polar molecule. According to our studies, $Cu_3(btc)_2$ is highly efficient for methane storage due to a trimodal pore size distribution. At lower pressure, the smaller pores and, as we will show in this paper, the open metal centres result in strong interaction, whereas at higher pressure there is still room for increasing capacity due to the filling of the larger pore. Compared to other MOF

* Corresponding author. Address: Department of Inorganic Chemistry, Technical University of Dresden, Mommsenstr. 6, D-01062 Dresden, Germany. Tel.: +49 351 46334885; fax: +49 351 46337287.
E-mail address: stefan.kaskel@chemie.tu-dresden.de (S. Kaskel).

1387-1811/$ - see front matter © 2010 Elsevier Inc. All rights reserved.
doi:10.1016/j.micromeso.2010.07.020

materials, $Cu_3(btc)_2$ also has a high volumetric adsorption capacity. The latter indicates efficient packing of methane inside the pores.

2. Experimental

2.1. Preparation of $Cu_3(btc)_2$

$Cu_3(btc)_2$ was synthesized by the method described previously [8]. The product was dried at 423 K and evacuated at 453 K for 24 h. The crystallinity and the purity of the product are examined via X-ray powder diffraction analysis.

2.2. Adsorption study

The pore volume of the synthesized sample was determined from N_2 adsorption isotherm measured at 77 K. The high-resolution methane adsorption isotherms were measured at 77 K and 87 K using a Quantachrome Autosorb1C apparatus equipped with cryostat (Oxford) on 14 mg of sample. To prevent condensation of CH_4 the pressure range was below 13.20 mbar at 77 K and below 18.67 mbar at 87 K. High pressure methane adsorption at several temperatures (285–373 K) was studied using a magnetic suspension balance (Rubotherm). The buoyancy correction was performed by a procedure published earlier [8]. Methane of 99.95% purity was used for the high pressure adsorption experiments and 99.99% purity for low pressure adsorption experiments. Prior to all adsorption measurements the sample was evacuated at 453 K for 16 h. For the calculations, the following values are used: $M(CH_4) = 16.043\ g\ mol^{-1}$, $V(CH_4)$ (STP: 273 K, 1 bar) = 22657 $cm^3\ mol^{-1}$, $M(Cu_3(btc)_2) = 604.92\ g\ mol^{-1}$.

2.3. In situ gas adsorption neutron diffraction experiment

The experiments were carried out at E9 diffractometer of Helmholtz Centre Berlin for Materials and Energy. The measurement cell was constructed of aluminum alloy because it has a small cross-section for neutron scattering. The at 353 K pre-activated sample (1.148 g) was pleased into the measurement cell under argon atmosphere in a glove box and activated again at 453 K for eight hours before the experiment was started. During the experiments, a dose amount of CD_4 gas (Sigma Aldrich, 99% atom % D) was loaded into the sample cell, and maintained at a temperature of 77 K for 2 h to reach the equilibrium state. A radiation with wavelength of 2.8160 Å was chosen for the dada collection. The data were collected at 77 K in 2Theta range between 8.00 and 156.026° with a step width of 0.078114°. The refinement of the measurements was carried out with the WinPlotR program package [16]. CD_4 was refined as a rigid body, a tetrahedron with d(C–D) = 1.09 Å. The topology of the networks has been examined with program package TOPOS [17] and *Gavrog Systre* [18].

2.4. Molecular simulation methods and models

Methane adsorption in $Cu_3(btc)_2$ was studied using grand canonical Monte Carlo (GCMC) simulations implemented in the multipurpose simulation code MUSIC [19]. In the grand canonical ensemble, the chemical potential, the volume and the temperature are kept fixed as in adsorption experiments. In the simulation, molecules were randomly moved, inserted and deleted which allowed the number of molecules in the framework to fluctuate. This method was also used to simulate the siting of CH_4 at 77 K as allowing the number of molecules to fluctuate through random insertions and deletions rather than keeping the number of molecules fixed, allowed a much more efficient exploration of the favorable sites within the $Cu_3(btc)_2$ framework. The siting simulations were carried out at pressures that resulted in average loading corresponding to the experimental loadings.

An atomistic model was used for the $Cu_3(btc)_2$ framework with the atoms kept fixed at the crystallographic positions [20]. The standard 12–6 Lennard–Jones (LJ) potential was used to model all interatomic interactions. The parameters for the framework were obtained from the UFF force field [21]. The model used for methane was derived by Goodbody et al. from vapor liquid equilibrium data and uses a united-atom description of the methane molecules, i.e. one methane molecule was represented by a single sphere ($\sigma_{CH_4} = 3.730$ Å, $\epsilon_{CH_4}/k_B = 148.000$ K). The Lorentz–Berthelot mixing rules were employed to calculate the mixed methane/framework parameters. Interactions beyond 18.650 Å were neglected. 3×10^7 Monte Carlo steps were performed, carefully ensuring that equilibrium was reached. The first 40% were used for equilibration, and the remaining steps were used to calculate the ensemble averages.

GCMC simulations were also performed to determine the adsorbate loadings, n_{abs}, for pressures (p) ranging to 300 bar for temperatures, T = 285, 303, 333, 353, and 373 K. The excess amount of CH_4 adsorbed, n_{excess}, is given by

$$n_{excess} = n_{abs} - \frac{pV_{pore}}{ZRT} \quad (1)$$

where Z is the compressibility factor. The Peng–Robinson equation of state was used to estimate Z. The accessible pore volume within the crystals, V_{pore}, was taken to be equal to experimentally determined value of 0.72 $cm^3\ g^{-1}$.

3. Results and discussion

3.1. Structure

$Cu_3(btc)_2$ crystallizes in the cubic space group *Fm-3m* and has a three-dimensional twisted boracite framework (**tbo**) (Fig. 1) composed of binuclear copper paddle-wheel units bridged by three-connecting btc ligands [22]. The framework contains three different types of pores. One of them is relatively small (further denoted as S1 pore) with a diameter of 5 Å (diameter in this text is calculated as twice the distance between the center of the pore and the center of the benzene ring minus twice the van der Waals radius of a carbon atom of 1.7 Å). One unit cell includes 8 such small pores with the center in 0.25, 0.25, 0.25 (Wyckoff notation 8c), which can be compared with the tetrahedral holes of a faced center cubic packed structure (Fig. 1a, 1b). Additionally larger pores (L2) in 0.5, 0.5, 0.5 (Wyckoff notation 4b) are present, representing the octahedral holes of an fcc structure. The diameter is about 11 Å (calculated as described above). The inner surface of the pore is constructed from benzene rings of the trimesic acid with the 6-fold axis of the rings pointing towards the pore center (Fig. 1c). The third type of pores (L3) with round about 13.5 Å in diameter (calculated as twice the distance between the center of the pore and the copper atom minus twice the van der Waals radius of copper (1.4 Å)) is located in 0.0, 0.0, 0.0 (Wyckoff notation 4a). In contrast to L2, the benzene rings do not form the inner surface but the hydrogen atom of the trimesic linker point towards the pore center (Fig. 1d). Only L3 pores have open copper coordination sites pointing into the pore. The pore sizes determined from the crystal structure agree well with the pore sizes calculated with the method developed by Gelb and Gubbins (Fig. 2), which determines the diameter of the largest sphere that can fit into the cavities without overlapping with any of the framework atoms [23]. The pore diameter for the small S1 pores is 4.9 Å and diameters for the large pores L2 and L3 are calculated to be 10.5 and 12.2 Å, respectively.

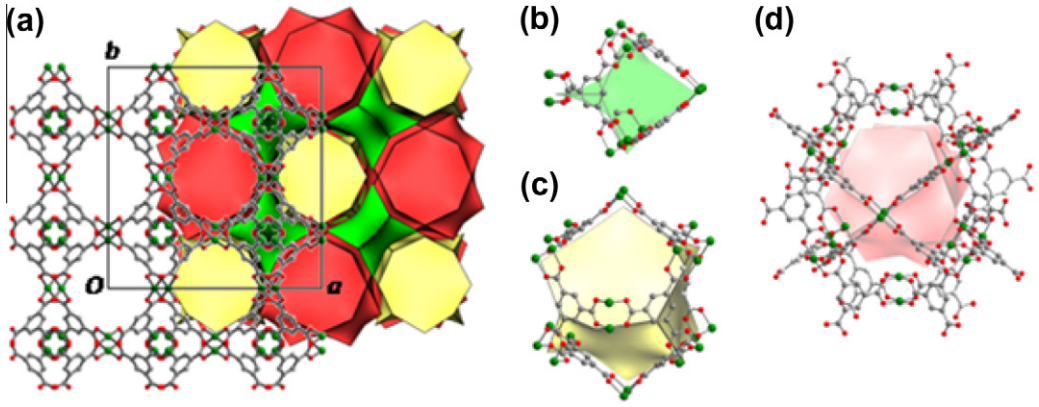

Fig. 1. (a) View on the structure of $Cu_3(btc)_2$ along *c*; (b) small pores (S1) (eight per unit cell); (c) large pore (L2) (four per unit cell); (d) large pore (L3) (four per unit cell). Carbon atoms are drawn in grey, copper in green, oxygen in red. (For interpretation of the references in colour in this figure legend, the reader is referred to the web version of this article.)

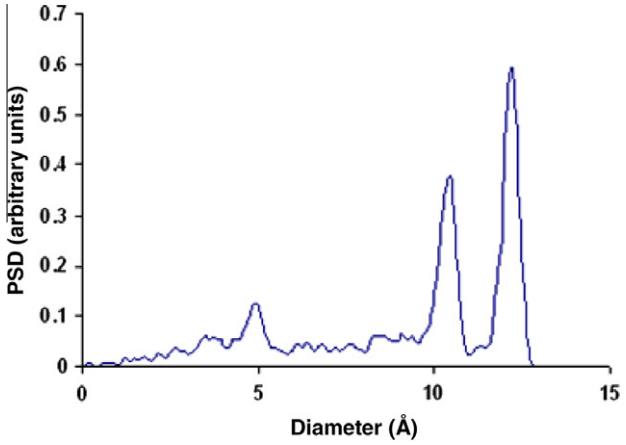

Fig. 2. Pore size distribution (PSD) for $Cu_3(btc)_2$.

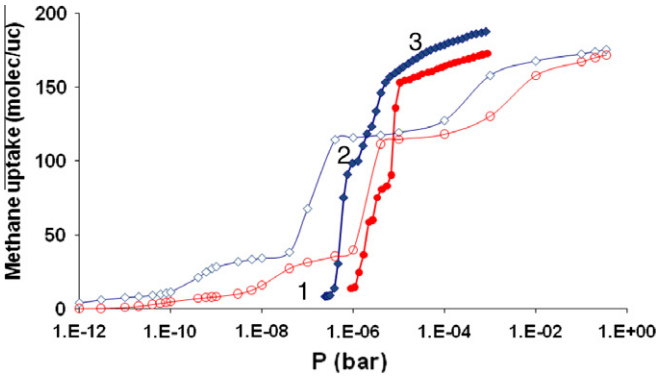

Fig. 3. Experimental (closed symbols) and simulated (open symbols) low pressure methane adsorption isotherms for $Cu_3(btc)_2$ at 77 K (diamond) and 87 K (circle) drawn in logarithmic scale. The loadings 1, 2, and 3 calculated from the isotherm and used during the *in situ* experiments are pointed.

3.2. Gas adsorption

Analysis of the nitrogen adsorption isotherm measured at 77 K revealed for the $Cu_2(btc)_2$ sample a pore volume of 0.72 $cm^3\ g^{-1}$. This result is in fair agreement with the values published before [24].

Methane adsorption isotherms obtained from both experiments and simulations for $Cu_3(btc)_2$ at 77 and 87 K are shown in Fig. 3, drawn in a logarithmic scale to better show the adsorption behavior at low pressures. The experimental isotherms in Fig. 3 exhibit distinct steps. Similar stepwise isotherms were previously observed also for low temperature nitrogen and argon adsorption [25,26]. It should be noted that when drawn on a linear scale the isotherms appear to be type I. Yet, the steps in the isotherms clearly demonstrate that the adsorption mechanism is more complex. For methane, the first step observed at 5×10^{-6} bar and 87 K corresponds to a loading of 200 cm^3(STP) g^{-1} which is equivalent to 85 molecules per unit cell whereas for experimental argon isotherms this step corresponds to a loading of about 90 cm^3(STP) g^{-1} or 38 molecules per unit cell [26]. This difference between argon and methane adsorption indicates the importance of open metal sites for methane adsorption: while the first step for argon adsorption corresponds to a filling of the small S1 pores which can accommodate 40 molecules per unit cell (one in the centre and one in each of the four windows of the eight S1 pores), the step in the methane isotherm points towards a combination of filling the small pores and occupying the 48 open metal sites in the L3 pores. The same is observed for nitrogen adsorption in $Cu_3(btc)_2$ [25]. For pressures larger than 5×10^{-6} bar, a gradual filling of the large pores L2 and L3 pores occurs up to a maximum loading of 416 cm^3(STP) g^{-1} at 87 K.

Whereas the simulations reproduce of the experimental step around 110 mol/uc, they also predict the existence of additional steps (one at low pressure and another at high pressure) that are not found experimentally (compare Fig. 3). These additional steps were also observed for simulated argon adsorption isotherms in $Cu_3(btc)_2$ [26]. These differences indicate that part of the complex experimental adsorption mechanism is not captured correctly by the GCMC simulations. In the simulations, methane molecules first occupy the centres and the windows of the small S1 pores corresponding to the first two steps. This is followed by the filling of L2 pores (third step) and, finally, the filling of L3 combined with a reordering of methane molecules in the cavities (fourth step). As discussed in greater detail later, neutron diffraction shows the existence of adsorption sites at the exposed metal sites in L3 (48 positions per unit cell) which are not captured by the GCMC simulations.

The loading 1 for the *in situ* gas adsorption neutron diffraction experiment is 8 CH_4 molecules per unit cell, loading 2 corresponds to 104 CH_4 molecules per unit cell of $Cu_3(btc)_2$ or about 59% of the saturation loading. The amount of gas for the loading 3 corresponds to the complete filling of the $Cu_3(btc)_2$ pores with methane. This amount is equal to 176 methane molecules per unit cell of $Cu_3(btc)_2$.

In addition to the low pressure/low temperature adsorption study the high pressure methane adsorption isotherms were measured in the temperature range from 285 to 373 K (Fig. 4).

GCMC simulations were also performed to determine the adsorbate loadings for pressures ranging to 300 bar for temperatures, T = 285, 303, 333, 353, and 373 K. Fig. 4b shows the comparison of the simulated and experimental values of n_{excess}. The deviations between experiments and simulations are particularly sensitive to the chosen value of V_{pore} and also the estimations of the compressibility factor Z. Nevertheless, a reasonably good agreement between the two sets is obtained for the range of pressures up to 200 bar. The experimental data only extend to 200 bar, but the simulations were carried out to 300 bar. As p = 300 bar is approached, the GCMC simulations show that the excess adsorption loadings for various temperatures tend to converge to the same value, and this trend is in line with experimental data. In storage applications the choice of the optimum temperature and pressure are both important. If the excess adsorption is independent of temperature for p = 300 bar, this would imply that there is no need to optimize for the temperature conditions.

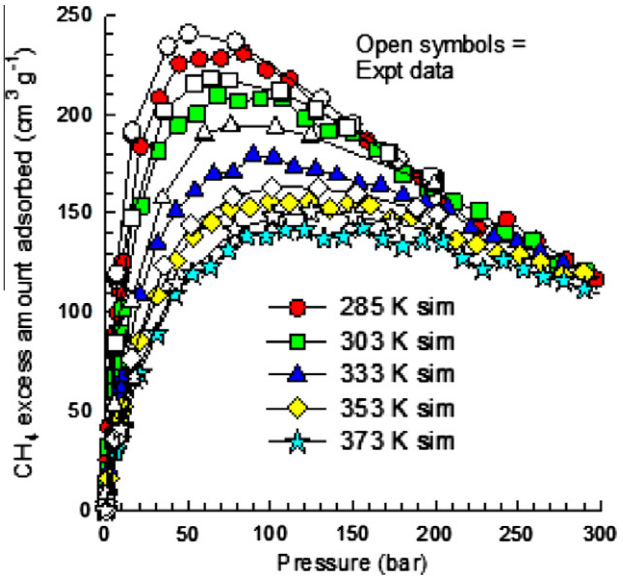

Fig. 4. Comparison of experimental excess loadings (open symbols) with GCMC simulations (filled symbols).

3.3. Crystallographic results

To get a good starting model, in a first step the atoms positions of the activated framework without gas molecules were refined. The latter is necessary because the activation and solvent removal causes a subtle change in the Cu–Cu distance in the compound. In the refinement by Chui et al. [22], the Cu–Cu paddle wheel still coordinates one water molecule per copper with a Cu–Cu distance of 2.628(2) Å. The activated structure, according to our neutron refinement, has a somewhat shorter Cu-Cu distance of 2.4137(1) Å and the positional parameters of O and C atoms are slightly relaxed (see Supplementary material).

In the subsequent refinements of the structure with adsorbed molecules, positional parameters and the B_{Iso} values of the framework atoms were fixed, in order to achieve a stable refinement of the various CD_4 loadings and the B_{Iso} values of the CD_4 atoms were fixed to 1.5.

A comparison of the neutron powder patterns of the empty framework with the completely filled material (Fig. 5) demonstrates the strong contribution of the guest molecules (CD_4) to the changes of the scattering intensities especially between 35 and 60°, whereas the peak location is not significantly changed and new peaks are not observed.

$Cu_3(btc)_2$ is a rather rigid metal-organic framework with a highly porous and inflexible framework. The structure was originally refined using single crystal X-ray data in the space group *Fm-3m* (a = 26.343(5)) Å [22]. According to our *in situ* neutron study, the framework remains intact without change of structure upon methane filling. Thus with higher degree of filling, a slight decrease of the lattice parameter is observed from 26.282(1) Å to 26.276(1) Å leading to a slight volume contraction of the cell (Table 1) Similar observations were made during the D_2 adsorption

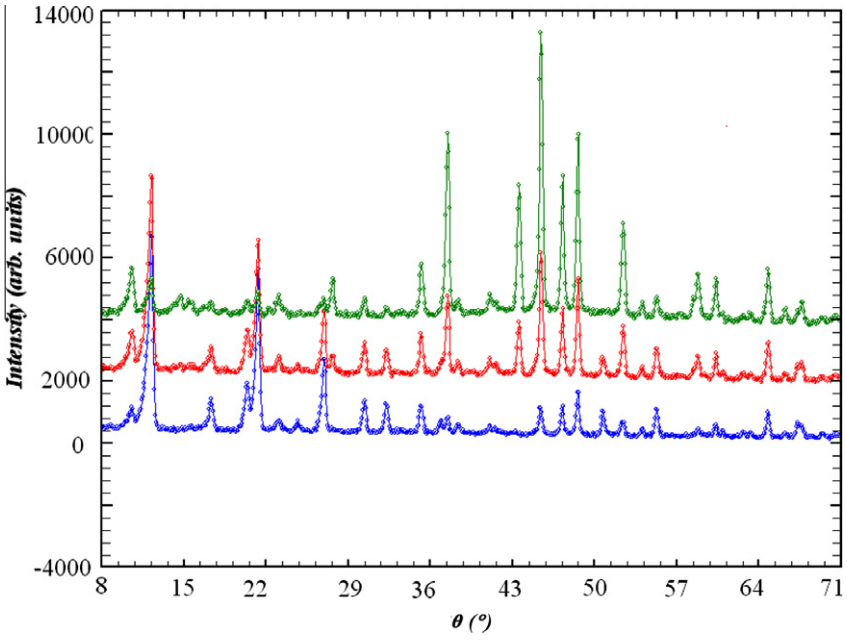

Fig. 5. Section of the measured neutron diffractograms between 3 and 73°: bottom: evacuated $Cu_3(btc)_2$; middle: $Cu_3(btc)_2$ loaded with around 59% CD_4 (104 mol/uc); at the top: complete filling with CD_4 (176 mol/uc).

Table 1
The cell parameters and cell volume of $Cu_3(btc)_2$ calculated for different gas loadings.

	Molec CD_4 /uc	% of maximal loading	Cell parameter a (Å)	Volume of the unit cell (Å^3)
$Cu_3(btc)_2$ empty	0	0	26.2821(3)	18154.4(3)
Loading 1	8	4.5	26.2824(3)	18154.9(3)
Loading 2	104	59	26.2795(2)	18148.9(3)
Loading 3	176	100	26.2762(4)	18142.2(5)

on $Cu_3(btc)_2$ [10]. We note in passing that this minimal change in the unit cell volume (less than 0.07%) confirms that the assumption of keeping the framework atoms fixed in the simulation is valid.

Only for the framework filled completely with CD_4, we were able to localize guest molecules in all three pores and at the windows between them. The refinement leads to eight different sites for the CD_4 molecules. Four main adsorption sites and four secondary sites can be distinguished with respect to the number of molecules per cell resulting from their occupation (Table 2). For the main adsorption sites, one is located in each pore (sites *A*, *B*, *C*) and one at the window between the large pores (site *D*).

The occupancy of the sites was refined to estimate the number of molecules adsorbed in each site. In total, we found ~31 and ~140 molecules per unit cell in the small and large pores, respectively.

In the small pore S1, the sites *A* and *E* are occupied. *E* is located at the center of the pore and the adjacent main site *A* (see above) is closer to the center of the window (1.30 Å) to the larger pores (Fig. 6a). Both sites are also observed in the simulations.

The distance between site *A* (S1 pocket) and site *G* (S1-L3) is 1.9 Å. Taking into account the diameter for CH_4 (3.74 Å) it should be remarked, that site *A* and *G* cannot be occupied simultaneously in the same pocket. The shortest distance for site *B* (located in L2 and illustrated in Fig. 6b) to the host framework obtained experimentally is about 4.36 Å (to the center of the benzene ring of the btc-ligand) and the distance to the copper ion is about 5 Å, which agrees well with the distances predicted by simulations (4.35 Å and 5.04 Å, respectively).

In the large pore L3, the main adsorption site obtained experimentally is site *C* located very close to the open metal sites. 44.6 mol/uc are observed at this loading at site *C*, which corresponds to 93% occupancy of the 48 open metal sites/unit cell. The CD_4 is located much closer to the copper ion than in the other large pore L2 (3.075 Å, see Fig. 7a). This distance is somewhat shorter than expected for physisorption. Yet, our adsorption studies demonstrated that adsorption is completely reversible meaning that despite the smaller distance, physisorption rather than chemisorption is taking place at the open metal sites. Similar values have been observed for methane adsorption on other MOFs with open metal sites [15] and could be caused by the high Lewis acidity of the open metal center, which might result in a polarization of the CD_4 molecules as observed for H_2 or CO [27]. As the distance is considerably smaller than half the mixed Lennard–Jones parameter for methane and copper ($0.5(\sigma_{Cu} + \sigma_{CH_4}) = 3.422$ Å), it cannot be reproduced by the GCMC simulations. An additional main adsorption site *D* is located close to the windows between L2

Table 2
Adsorption sites for loading 3 (complete pore filling, 176 mol/uc).

Site	Pore type	*X*	*Y*	*Z*	Occupancy	Molecules per unit cell
A	S1	0.1788(34)	0.1788(34)	0.1572(49)	0.132(6)	24.76
B	L2	0.8817(9)	0.5	0.8817(9)	0.25	48
C	L3	0.8845(17)	0.5	0.6599(17)	0.232(2)	44.63
D	L2–L3	0.5598(32)	0.2289(30)	0	0.146(5)	27.8
E	S1	0.25	0.25	0.25	0.0333(7)	6.39
F	L2-L3	0.293(20)	0	0	0.020(3)	4
G	S1–L3	0.132(15)	0.641(12)	0.641(12)	0.058(6)	11.76
H	L3	0	0	0	0.02083	4
Sum					0.891733	171.21
Calculated from the CD_4 amount loaded						176

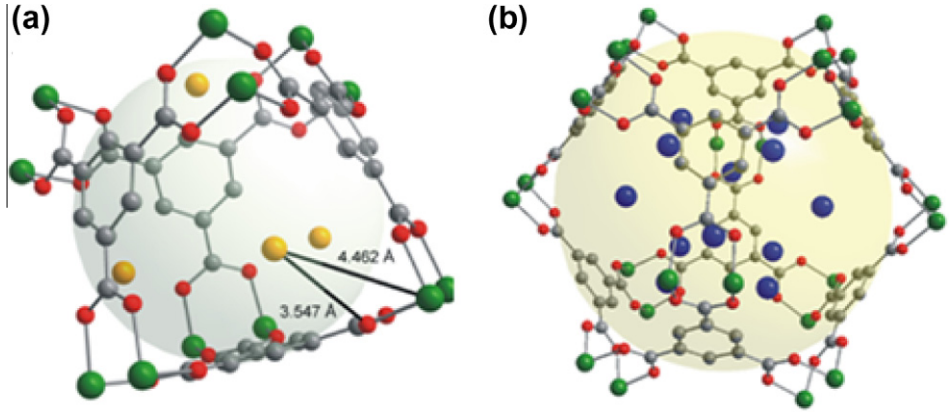

Fig. 6. (a) Small pore filled up with D_4-methane: the distance of the main adsorption site *A* (in orange) to the copper ion (green) and the shortest distance to oxygen (red) is shown (for clarity not all methane molecules are shown); (b) The main adsorption site in pore L2 (site *B*, see Table 1) in blue. Carbon atoms are drawn in grey. (For interpretation of the references in colour in this figure legend, the reader is referred to the web version of this article.)

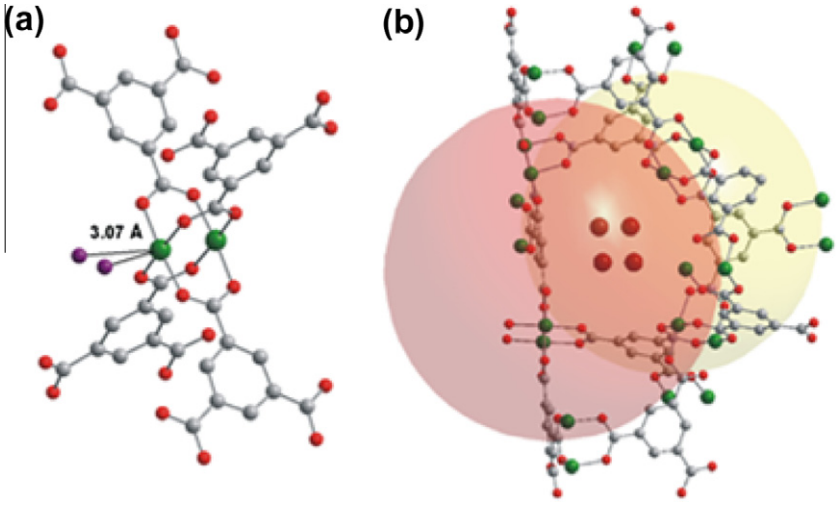

Fig. 7. (a) Main adsorption site *C* (violet) in the pore L3. The D_4-methane is located closer to the copper ion; (b) the main adsorption site *D* (in brown) is located at the window between pore L2 and L3. Carbon atoms are drawn in grey, copper in green, oxygen in red. (For interpretation of the references in colour in this figure legend, the reader is referred to the web version of this article.)

and L3 (see Fig. 7b). Finally, another secondary site *F* was found next to site D in the same window, and two more secondary sites were found in the center of larger cavity L3 (site *H*), and in between S1 and L3 (site *G*).

Refining the framework loaded with a small amount of methane (8 molecules per unit cell, loading 1) CD_4 was more difficult due to the dilution of scattering density at certain sites. Obviously the 100% loading corresponds to an optimized packing of a more localized structure, whereas at lower loading, a continuous description would be more appropriate. However, at the second adsorption loading (about 59% of the saturation loading or 104 mol/uc), we are able to locate the molecules on six different adsorption sites (Table 3). Four of them are main sites; the others contribute to the filling to a lesser extent.

The main sites are nearly the same as for the fully filled sample, only the occupancy decreases as expected. Additionally the center of the small pore (site *E*) is occupied by a small amount of CD_4 molecules and we are able to locate a small amount of CD_4 molecules near the center of the large pore L2 (site *I*). The other secondary adsorption sites of the loading 3 seem to be empty at this lower filling. In each small pore S1, approximately 2 molecules are detected, whereas ~15 molecules are located in each of large pores L2 and L3 with only 21.12 or 44% of the open metal sites occupied by CD_4 molecules. Observing the majority of molecules in the large pores is somewhat unexpected, since the higher interaction potential of the smaller pores and the open metal sites should lead to a sequential filling of the small pores and open metal sites, and larger pores, respectively. This discrepancy, the contrast between the 104 mol/uc loaded and ~67 mol/uc located, and the appearance of site *I* at the intermediate loading are signals for an incomplete equilibrium during the filling operation. Some adsorbed molecules do not occupy equilibrium positions but are frozen at sites with higher adsorption rate and accessibility. However, the general trend of a continuously increasing occupancy of the certain adsorption sites with increasing gas loading is well described by the neutron diffraction experiments.

3.4. Modeling

As mentioned above classical GCMC simulations are not capable of describing the adsorption on the open copper sites (site *C*) correctly but rather predict a sequential filling of the small and large pores with increasing pressure. Here, we present further simulation results in order to explain the differences between the experimental and simulated adsorption isotherms and mechanisms. The sitting of the methane molecules is mainly determined by the potential energy between methane molecules and the framework. At higher loadings, packing of the methane molecules inside the framework as well as methane–methane interactions plays an additional role. Fig. 8 shows contour plots of the potential energy for two different cross-sections of the $Cu_3(btc)_2$ framework. It illustrates how much stronger the interaction in the smaller, S1, cavities is compared to the larger L2 and L3 cavities. Whereas the potential energy is -22.73 kJ mol^{-1} in the centre of the small S1 cavities, it is only -4.04 and -1.99 kJ mol^{-1} in the centre of the large L2 and L3 pores, respectively.

We studied the location of methane molecules in the framework at four different uptakes which correspond to the steps observed in the simulated isotherms at 77 K (Fig. 3): 8, 32, 108 and 176 mol/uc. At a loading of eight molecules per unit cell (Fig. 9a),

Table 3
Adsorption sites for loading 2 (59% of saturation loading, 104 mol/uc).

Site	Pore type	*X*	*Y*	*Z*	Occupancy	Molecules per unit cell
A	S1	0.1686(18)	0.1686(18)	0.1686(18)	0.0605(12)	11.66
B	L2	0.8717(17)	0.5	0.8717(17)	0.1065(14)	20.51
C	L3	0.8479(25)	0.5	0.6140(26)	0.1101(16)	21.12
D	L2–L3	0.5501(56)	0.2323(48)	0	0.0479(16)	9.1
E	S1	0.25	0.25	0.25	0.0174(5)	3.36
I	L2	0.480(20)	0	0	0.0074(5)	1.44
Sum					0.35	67.19
Calculated from the amount of CD_4 loaded						104

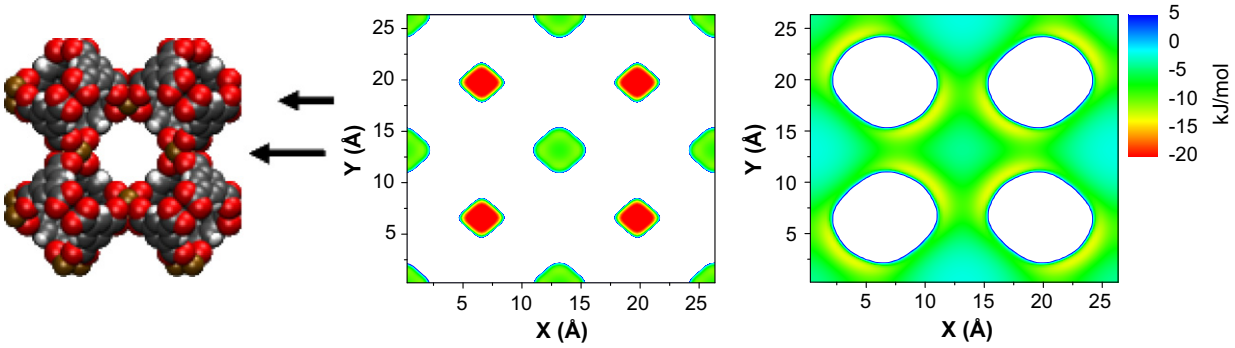

Fig. 8. Contour plots of the potential energy between a methane molecule and the $Cu_3(btc)_2$ framework on a plane through the centre of the small cavities (left), and on a plane through the centre of the large cavities (right). The white space corresponds to the $Cu_3(btc)_2$ framework.

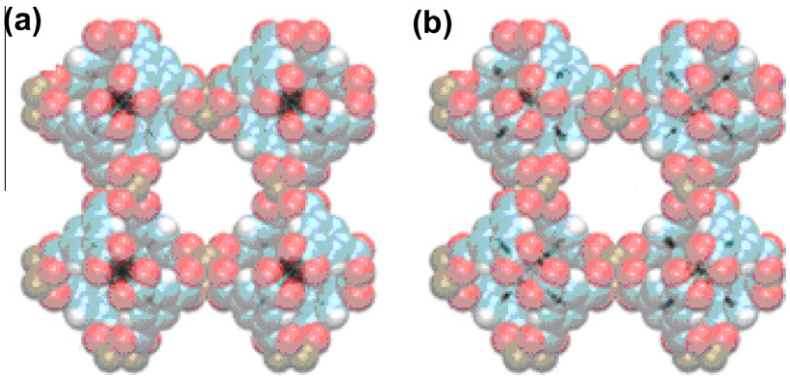

Fig. 9. Density distributions of methane on $Cu_3(btc)_2$ (75,000 configurations) at (a) 8 mol/uc and (b) 32 mol/uc. Each black dot represents the position of a methane molecule during the simulation. In total 75,000 configurations are shown.

the methane molecules are mostly located inside the small cavities (S1), i.e. site *E*; whereas for 32 mol/uc (Fig. 9b), the molecules are located not only inside these small cavities but also in the windows that connect small (S1) and large cavities (L3), i.e. site *A*. These molecules are forced into much more localized positions by the presence of more methane molecules as indicated by the confined positions in the density distribution in Fig. 9b. This is in contrast to the lower loading where the molecules can move much more freely in the smaller cavities as illustrated by the much wider black area that the molecules cover in Fig. 9a. Note that in both cases the same number of configurations (75,000) is represented.

Fig. 10 clearly shows that at the lowest loading (8 mol/uc) there are no molecules present in the larger cavities. The density profiles are fairly wide rather than localized at discrete points meaning that the molecules are free to move inside the smaller cavities (site *E*) without any further space limitation or methane-methane packing effects. This is very likely the reason for the dilution of the scattering density in the experiments and the resulting difficulties in refining of the neutron scattering pattern. When the loading increases to 32 mol/uc, the additional molecules in the windows of the small cavities (site *A*) constrain the adsorbed molecules of site *E* to a more fixed position to allow better packing (not shown).

At a loading of 104 mol/uc, methane molecules start filling the larger pores L2 (Fig. 10 predicting adsorption at sites *B*, *D*, *F* and *I*). Finally, at a loading of 176 mol/uc, methane continues with the pore filling of the large cavities, including site *H* in L3. No occupancy of site *C*, close to the open metal sites, was observed even for a loading of 176 mol/uc (compare Table 4). The much smaller extent of the individual regions shown in Fig. 10 as well as the change in their position indicates that a reordering of the methane molecules is taking place between 104 and 176 mol/uc. Moreover, the average distance between these clusters inside the large cavities changes from 4.09 Å to 3.73 Å where the latter corresponds to the Lennard–Jones parameter σ (i.e. the hard sphere diameter) for methane used in the simulations. This reordering of the molecules inside the cavities was not detected experimentally and, together with the existence of the non-predicted site *C* at L3, is the explanation of the last step in the simulated adsorption isotherm shown in Fig. 3 that is not observed in the experimental isotherm.

Finally, in order to elucidate these processes further, we calculated the energy histograms at different uptakes (Fig. 11), i.e. we determined the potential energy for each methane molecule with the framework during the simulation. Different peaks associated with the small (S1) and large (L2 and L3) pores are observed: the first one at -22.7 kJ mol^{-1} corresponds to the centre of S1 (site *E*); the second one at -19.6 kJ mol^{-1} is associated with the windows between small and large pores (site *A*), -12.9 kJ mol^{-1} is mainly associated with the windows between large pores and the filling of L2 (sites *B*, *D* and *F*); the last ones are associated with the large cavity L3 (-4.8 kJ mol^{-1}, site *H*) and the centre of L2 (-3.9 kJ mol^{-1}, site *I*). Note that, the lower the energy the stronger the interaction between methane and the framework. The energy histograms in Fig. 11 show that the adsorption mechanism starts with the filling of the centre (histogram for 8 mol/uc) and the windows (histogram for 32 mol/uc) of the small cavities, i.e. sites *E* and *A*, respectively. Then, the methane molecules start filling the sites with higher energies: at 104 mol/uc the methane are localized not only in the small pores (S1) but also in the larger cavities L2 and the windows between L2 and L3, i.e. sites *B*, *D*, *F* and *I*. Finally, at 176 mol/uc (Fig. 11, black triangle), methane goes into L3 cavities, i.e. site *H*. Although the strong interaction sites in S1 are occupied for each loading their importance diminishes with increased loading due to their limited number and less favorable sites gain more importance.

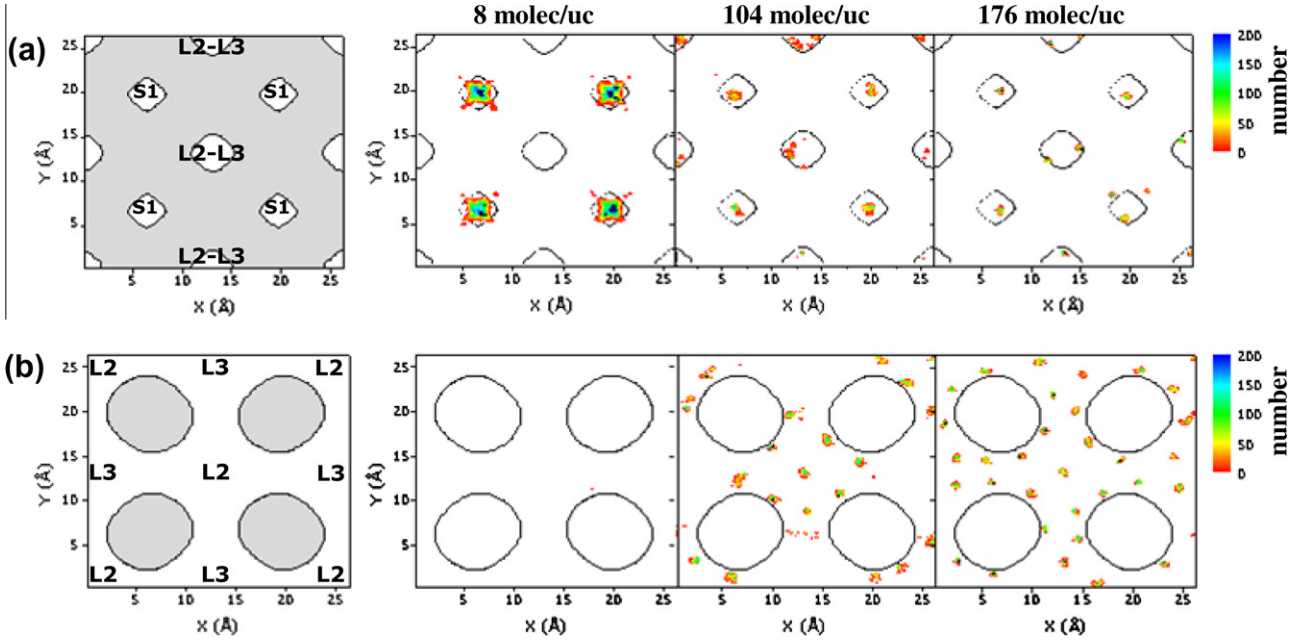

Fig. 10. (a) Location of the pores (white) and number distribution at different global uptakes of 176, 104, 32 and 8 mol/uc, (determined for a slice cut through S1). (b) Localization of the framework pores and number distribution determined for a slice cut through L2 and L3.

Table 4
Adsorption sites occupancy calculated for the different loadings (experimental results in brackets).

Site	Energy (kJ mol^{-1})	8 mol/uc	32 mol/uc	104 mol/uc (67.19 mol/uc)	176 mol/uc (171 mol/uc)
A	−19.6	15.1%	86.4%	29.7% (17.4%)	18.8% (21.33%)*
B, D, F	−12.9	0.0%	0.2%	60.5% (44%)	57.0% (46.5%)
C	N/A	0.0%	0.0%	0.0% (31.4%)	0.0% (26%)
E	−22.7	84.9%	13.6%	6.7% (5.0%)	3.5% (3.7%)
I	−3.9	0.0%	0.0%	3.0% (2.14%)	1.8% (0.0%)
H	−4.8	0.0%	0.0%	0.0% (0.0%)	18.9% (2.3%)

* The sum of occupancies of site *A* and site *G*.

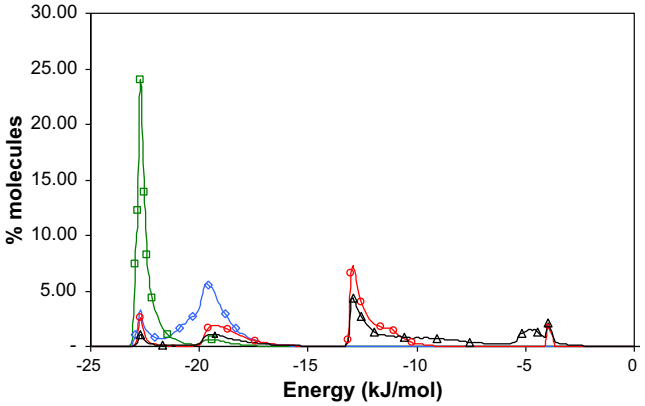

Fig. 11. (a) Energy histograms of methane on $Cu_3(btc)_2$ at 8 mol/uc (green square), 32 mol/uc (blue diamond), 104 mol/uc (red circle) and 176 mol/uc (black triangle). (For interpretation of the references in colour in this figure legend, the reader is referred to the web version of this article.)

4. Conclusions

In situ neutron diffraction was successfully used for the localization of methane (CD_4) in a model metal-organic framework, namely $Cu_3(btc)_2$. In the smallest pore of the framework, two distinct positions with fractional occupancy were identified, a central position and one at the pore window. In the large pores a complex packing of methane molecules is responsible for the high storage capacity in the MOF. Our results have demonstrated the important role of open metal sites even for the adsorption of methane, a non-polar and highly symmetrical molecule, resulting in highly attractive adsorption sites and distances between methane and copper that are smaller than expected for physisorption. This complex behavior is not captured by classical GCMC simulations (note, however, that DFT calculations have recently predicted this reduced distance for other MOFs with open metal sites [15]). The GCMC simulations predict a different adsorption mechanism based on sequential pore filling and reordering of the methane molecule. Consequently, the absence of an open metal site from simulation results does not necessarily mean that it does not play a role in the adsorption mechanism [9] but could well be caused by an artifact of the simulation method. Advanced experimental techniques such as *in situ* neutron diffraction or IR spectroscopy [28] combined with careful analysis of low temperature isotherms are clearly needed to further elucidate the role of open metal sites for different adsorbates and fully understand their role not only for gas storage but also separation.

Acknowledgement

We would like to thank BENSC (HZB) for neutron beam time and EC for financial support. D.F.-J. thanks the Universidad de Granada (Spain) for financial support.

Appendix A. Supplementary data

Crystallographic data (Table S1) and fractional atom coordinates (Table S2) for activated $Cu_3(btc)_2$, loaded with 104 molecules

CD_4 per unit cell (loading 2) and 176 mol/uc (loading 3), Rietveld plots of loading 2 (Fig. S1) and loading 3 (Fig. S2).

Supplementary data associated with this article can be found, in the online version, at doi:10.1016/j.micromeso.2010.07.020.

References

[1] M. Hirscher, B. Panella, Scripta Mater. 56 (2007) 809.
[2] U. Mueller, M. Schubert, F. Teich, H. Puetter, K. Schierle-Arndt, J. Pastre, J. Mater. Chem. 16 (2006) 626.
[3] R.E. Morris, P.S. Wheatley, Angew. Chem. Int. Ed. 47 (2008) 4966.
[4] S.S. Kaye, A. Dailly, O.M. Yaghi, J.R. Long, J. Am. Chem. Soc. 129 (2007) 14176.
[5] M. Dinca, J.R. Long, Angew. Chem. Int. Ed. 47 (2008) 6766.
[6] D. Zhao, D. Yuan, H.-C. Zhou, Energy Environ. Sci. 1 (2008) 222.
[7] B. Panella, M. Hirscher, H. Puetter, U. Mueller, Adv. Funct. Mater. 16 (2006) 520.
[8] I. Senkovska, S. Kaskel, Microp. Mesopor. Mater. 112 (2008) 108.
[9] E. Garcia-Perez, J. Gascon, V. Morales-Florez, J.M. Castillo, F. Kapteijn, S. Calero, Langmuir 25 (2009) 1725.
[10] V.K. Peterson, Y. Liu, C.M. Brown, C.J. Kepert, J. Am. Chem. Soc. 128 (2006) 15578.
[11] Y. Liu, C.M. Brown, D.A. Neumann, V.K. Peterson, C.J. Kepert, J. Alloys Compd. 446–447 (2007) 385.
[12] T. Yildirim, M.R. Hartman, Phys. Rev. Lett. 95 (2005) 215504/1.
[13] Y.S. Zhao, H.W. Xu, L.L. Daemen, K. Lokshin, K.T. Tait, W.L. Mao, J.H. Luo, R.P. Currier, D.D. Hickmott, Proc. Natl. Acad. Sci. USA 104 (2007) 5727.
[14] M.R. Hartman, V.K. Peterson, Y. Liu, S.S. Kaye, J.R. Long, Chem. Mater. 18 (2006) 3221.
[15] H. Wu, W. Zhou, T. Yildirim, J. Am. Chem. Soc. 131 (2009) 4995.
[16] T. Roisnel, J. Rodriguez-Carvajal, Mater. Sci. Forum 378–381 (2001) 118.
[17] V.A. Blatov, IUCr Compcomm Newsletter 7 (2006) 4.
[18] http://gavrog.sourceforge.net.
[19] A. Gupta, S. Chempath, M.J. Sanborn, L.A. Clark, R.Q. Snurr, Mol. Simul. 29 (2003) 29.
[20] B. Xiao, P.S. Wheatley, X. Zhao, A.J. Fletcher, S. Fox, A.G. Rossi, I.L. Megson, S. Bordiga, L. Regli, K.M. Thomas, R.E. Morris, J. Am. Chem. Soc. 129 (2007) 1203.
[21] A.K. Rappe, C.J. Casewit, K.S. Colwell, W.A. Goddard, W.M. Skiff, J. Am. Chem. Soc. 114 (1992) 10024.
[22] S.S.Y. Chui, S.M.F. Lo, J.P.H. Charmant, A.G. Orpen, I.D. Williams, Science 283 (1999) 1148.
[23] L.D. Gelb, K.E. Gubbins, Langmuir 15 (1999) 305.
[24] J. Liu, J.T. Culp, S. Natesakhawat, B.C. Bockrath, B. Zande, S.G. Sankar, G. Garberoglio, J.K. Johnson, J. Phys. Chem. C 111 (2007) 9305.
[25] P. Krawiec, M. Kramer, M. Sabo, R. Kunschke, H. Froede, S. Kaskel, Adv. Eng. Mater. 8 (2006) 293.
[26] A. Vishnyakov, P.I. Ravikovitch, A.V. Neimark, M. Bulow, Q.M. Wang, Nano Lett. 3 (2003) 713.
[27] C. Prestipino, L. Regli, J.G. Vitillo, F. Bonino, A. Damin, C. Lamberti, A. Zecchina, P.L. Solari, K.O. Kongshaug, S. Bordiga, Chem. Mater. 18 (2006) 1337.
[28] J.G. Vitillo, L. Regli, S. Chavan, G. Ricchiardi, G. Spoto, P.D.C. Dietzel, S. Bordiga, A. Zecchina, J. Am. Chem. Soc. 130 (2008) 8386.